HHS Public Access

Author manuscript

Neurobiol Dis. Author manuscript; available in PMC 2019 June 01.

Published in final edited form as:

Neurobiol Dis. 2018 June ; 114: 31–44. doi:10.1016/j.nbd.2018.02.006.

Frontotemporal dysregulation of the SNARE protein *interactome* is associated with faster cognitive decline in old age

Alfredo Ramos-Miguel[a,b], **Andrea A. Jones**[a,b], **Ken Sawada**[c], **Alasdair M. Barr**[a,d], **Thomas A. Bayer**[e], **Peter Falkai**[f], **Sue E. Leurgans**[g], **Julie A. Schneider**[g], **David A. Bennett**[g], and **William G. Honer**[a,b,*]

[a]BC Children's Hospital Research Institute, 938 West 28th Avenue, Vancouver, BC, V5Z 4H4, Canada.

[b]Department of Psychiatry University of British Columbia, 2255 Wesbrook Mall, Vancouver, BC, V6T 2A1, Canada.

[c]Kochi Medical School, Kohasu, Oko-cho, Nankoku, Kochi, 783-8505, Japan.

[d]Department of Anesthesiology, Pharmacology and Therapeutics, University of British Columbia, 2176 Health Sciences Mall, Vancouver, BC, V6T 1Z3, Canada.

[e]Department of Psychiatry, University Medicine Goettingen, von-Siebold-Strasse 5, D-37075 Goettingen, Germany.

[f]Department of Psychiatry and Psychotherapy, Ludwig-Maximilians-University Munich, Nussbaumstrasse 7, D-80336 Munich, Germany.

[g]Rush Alzheimer's disease Center, Rush University Medical Center, 600 S. Paulina Street, Chicago, IL 60612

Abstract

The molecular underpinnings associated with cognitive reserve remain poorly understood. Because animal models fail to fully recapitulate the complexity of human brain aging, postmortem studies from well-designed cohorts are crucial to unmask mechanisms conferring cognitive

[*]**Corresponding author at:** Department of Psychiatry, University of British Columbia, 2255 Wesbrook Mall, Vancouver, BC, Canada, V6T 2A1. william.honer@ubc.ca (WG Honer).

Author contributions

The present study was designed by WGH, DAB, AR-M and AMB. AR-M performed all experiments involving the characterization and quantification of presynaptic complexes in human brain tissues. KS assessed the immunohistochemical and immunofluorescence assays in human brain sections. DAB and JAS conceived the Rush Memory and Aging Project, performed all clinical and pathological exams, and procured human tissue samples. SEL compiled all participants' demographic, clinical and pathological data and, with the collaboration of AR-M, AAJ and WGH, run all statistical analyses. AR-M, AAJ and WGH wrote the first draft of the manuscript. All authors critically contributed to the discussion of the results and approved the final version of the manuscript.

DECLARATION OF INTEREST

WGH has received consulting fees or sat on paid advisory boards for: In Silico, Lundbeck/Otsuka, Eli Lilly, and Roche. AMB is on the advisory board or received consulting fees from Roche Canada, and received educational grant support from BMS Canada. The Organizations cited above had no role in (and therefore did not influence) the design of the present study, the interpretation of results, and/or preparation of the manuscript. All other authors have no financial interest on the reported data and declare that no competing interests exist.

resistance against cumulative neuropathologies. We tested the hypothesis that functionality of the SNARE protein *interactome* might be an important resilience factor preserving cognitive abilities in old age. Cognition was assessed annually in participants from the Rush 'Memory and Aging Project' (MAP), a community-dwelling cohort representative of the overall aging population. Associations between cognition and postmortem neurochemical data were evaluated in functional assays quantifying various species of the SNARE (soluble *N*-ethylmaleimide-sensitive factor attachment protein receptor) machinery in samples from the inferior temporal (IT, $n = 154$) and middle-frontal (MF, $n = 174$) gyri. Using blue-native gel electrophoresis, we isolated and quantified several types of complexes containing the three SNARE proteins (syntaxin-1, SNAP25, VAMP), as well as the GABAergic/glutamatergic selectively expressed complexins-I/II (CPLX1/2), in brain tissue homogenates and reconstitution assays with recombinant proteins. Multivariate analyses revealed significant associations between IT and MF neurochemical data (SNARE proteins and/or complexes), and multiple age-related neuropathologies, as well as with multiple cognitive domains of MAP participants. Controlling for demographic variables, neuropathologic indices and total synapse density, we found that temporal 150-kDa SNARE species (representative of pan-synaptic functionality) and frontal CPLX1/CPLX2 ratio of 500-kDa heteromeric species (representative of inhibitory/excitatory input functionality) were, amongst all the immunocharacterized complexes, the strongest predictors of cognitive function nearest death. Interestingly, these two neurochemical variables were associated with different cognitive domains. In addition, linear mixed effect models of global cognitive decline estimated that both 150-kDa SNARE levels and CPLX1/CPLX2 ratio were associated with better cognition and less decline over time. The results are consistent with previous studies reporting that synapse dysfunction (i.e. dysplasticity) may be initiated early, and relatively independent of neuropathology-driven synapse loss. Frontotemporal dysregulation of the GABAergic/glutamatergic stimuli might be a target for future drug development.

Keywords

SNARE complex; protein-protein interactions; native PAGE; postmortem brain; synaptic pathology; Alzheimer's disease; cognitive decline; excitatory/inhibitory balance; aging; double dissociation

Introduction

Cognitive impairment is a major health threat in the elderly. Age-related cognitive decline is associated with higher rates of disability, institutionalization, and mortality [1–4]. The neurological causes of cognitive impairment are diverse, accumulating and combining throughout the lifespan, with associated comorbidities [5]. Previous community-based studies attempted to estimate the extent of cognitive impairment and/or decline accounted for by multiple brain pathologies [5–9]. Combined, Alzheimer's disease (AD) pathology (i.e. senile plaques and neurofibrillary tangles), cerebrovascular diseases (including macro and microinfarcts), and Lewy body disease –the most common neuropathologies– could only explain 41% of between-subject variance in cognitive decline rates [7]. This incomplete predictive power is likely due to (1) subjects without known pathology whose cognitive function declined, and (2) subjects with pathologic burden who remained cognitively healthy

by the time of death. While the former might be explained by underestimated or yet unknown pathologies, the latter is typically attributed to cognitive reserve. Thus, cognitive reserve is commonly referred to as the individual's capacity to maintain cognition despite the increasing accumulation of pathologic lesions. In actuality, one can have more or less reserve; in the latter case, one would be more vulnerable to cognitive loss from neuropathology.

Synapses are considered core components of brain (and thereby cognitive) reserve [10]. Postmortem brain studies documented abnormally low numbers of dendritic spines in AD compared to age-matched healthy individuals [11], and loss of synapse density (including loss of several presynaptic proteins) was highly associated with cognitive impairment [12–15]. Similarly, several synaptic markers (such as synaptophysin) were found downregulated in AD brains [16,17]. In contrast, recent large-scale, community-based studies analyzing cohorts representative of the overall aging population with mixed pathologies documented that pan-synaptic loss may only occur following widespread accumulation of pathology; quantitative data estimating overall synapse density did not correlate well with ante-mortem cognitive scores after controlling for neuropathology [18,19]. These studies, however, showed that cognitive skills might be highly sensitive to variations in specific components of the neurosecretion machinery. For example, the amounts of binary interactions between the three well-known SNARE (soluble *N*-ethylmaleimide-sensitive factor attachment protein receptor) proteins, syntaxin-1, synaptosomal-associated protein-25 (SNAP25), and vesicle-associated membrane protein (VAMP, or synaptobrevin) [20,21], were highly associated with cognitive function nearest death [18]. Remarkably, the contribution of SNARE dysregulation to cognitive impairment was relatively independent from the neuropathologic burden [7]. Therefore, the network of protein-protein interactions (herein referred to as the "interactome") of the SNAREs, arguably a fingerprint of synaptic functionality by the time of death [22], might represent a different component of cognitive reserve.

The synaptic pool associated with brain reserve and cognitive decline is not homogenous across terminal types. In the same community sample, selective GABAergic variants of two key SNARE modulators, munc18–1a and complexin-I, were strongly correlated with cognitive performance, whereas the respective non-GABAergic species, munc18–1b (ubiquitous) and complexin-II (enriched in glutamatergic terminals), did not show comparable associations [23,24]. Remarkably, while GABAergic dysfunction had greater impact on cognitive performance in early stages, glutamatergic (or perhaps pan-synaptic) damage appeared relevant only after widespread accumulation of AD pathology (as assessed by Braak and CERAD rating scales), suggesting that failure of brain inhibitory system precedes spread of neuropathology [24]. Inhibitory-related brain reserve and its dysregulation may develop during brain maturation, as cortical loss of inhibitory markers was greater in carriers of the rs3846455 polymorphism in *UNC5C* gene [25]. *UNC5C* encodes for netrin receptor-1, a crucial molecule for axonal guidance and synaptogenesis, and the variant was found significantly associated with greater vulnerability to age-related pathology and poorer cognitive reserve [25,26].

We hypothesized that the SNARE interactome, and hence synaptic functionality, is a meaningful component of brain reserve, relatively independent from pathology-driven

synapse loss. To address this hypothesis, we quantified multiple protein complexes of the presynaptic machinery in postmortem brain samples from temporal and frontal lobes (pathologically affected at different stages) of participants in the community-based Memory and Aging Project (MAP) [27]. The SNARE interactome was characterized and quantified using non-denaturing, blue-native (BN) gels, preserving intact protein complexes [28,29]. The primary goal was to identify the major synaptic indices driving cognitive decline in MAP participants, and to estimate the extent of their contribution(s). For exploratory purposes, quantitative data was also integrated with multiple measures obtained in previous studies, including clinical, pathologic and stereological data.

Material and methods

Participants and cognitive evaluations

All samples were from The Rush Memory and Aging Project (MAP) [30]. MAP recruits community-dwelling volunteers within the metropolitan area of Chicago, IL, with no overt signs of cognitive impairment at study entry. Participants consented to annual clinical evaluations and signed an Anatomic Gift Act for organ donation upon death. All protocols in the study were reviewed and approved by the Institutional Review Board of Rush University Medical Center. The present study included postmortem brain samples collected in consecutive autopsies from 188 MAP participants. The relevant demographic, cognitive and pathological characteristics of the MAP participants studied appear in Table 1.

From enrollment to death (mean: 5.3 years; range: 2–12 years), a wide variety of cognitive and psychological outcomes were tracked [30]. Briefly, participants performed 21 cognitive tests annually, 19 of which were used to compile 5 different domains of cognition: episodic memory, semantic memory, working memory, perceptual speed or visuospatial ability. Scores within each domain were standardized (against baseline average values) and the mean across the domains was used as an estimate of participant's global cognitive function at that time point [30]. Mini-mental score examination (MMSE) scores were documented for comparisons with other studies (see Table 1). Clinical diagnoses of dementia followed the National Institute of Neurological and Communicative Disorders and Stroke and the AD and Related Disorders Association criteria [31], and were made by a board-certified neurologist blind to all pathological data.

Human brain specimens and neuropathological assessments

Strict standard procedures were followed at participants' autopsies to minimize between-subject variability and postmortem intervals (PMI) [30]. At autopsies, brains were quickly weighted, cut into 1-cm-thick coronal slabs, and photographed for gross neuropathology inspection. Hemispheres were segregated and either fixed in 4% paraformaldehyde for histopathological assessments or frozen at –80 °C for immunoassays. Tissue blocks containing key brain areas were obtained from the fixed brain slabs, paraffin-embedded and microtome-sliced into 6-μm-thick sections. [30].

A board-certified neuropathologist performed all neuropathological examinations, blind to participants' clinical data, and according to standard criteria [27,32]. The examinations

documented AD-related pathology, vascular diseases (macroscopic and microscopic infarcts, and arteriolosclerosis), Lewy bodies, and hippocampal sclerosis. In depth exploration for AD pathology reported (1) area fractions immunolabeled with amyloid-β (6F/3D or 4G8) and hyperphosphorylated tau (AT8) antibodies, and (2) stereological counts of neuritic and diffuse plaques, and neurofibrillary tangles (NFTs) as stained by a modified Bielchowsky's method [32]. A composite measure of global AD pathology was further obtained averaging the standardized scores of amyloid-β and tau loads across various key brain regions [33]. AD pathology was additionally graded using Braak staging, CERAD or NIA/Reagan scales [34–36]. Stereological studies of resting, activated or total microglial cells were reported earlier [37].

For the quantitative assessments of the present study, we used available frozen grey matter samples from the inferior temporal [IT; Brodmann's area (BA) 20; $n = 155$] and/or middle-frontal (MF; BA46/9; $n = 174$) gyri (see Table 1). These brain areas were selected based on their central role in cognitive processing and their contribution to the pathophysiology of age-related dementias [38]. Of note, spread of AD pathology through temporal and frontal cortices is typically used to stage the illness [34]. The dissected brain samples were solubilized in pre-chilled phosphate-buffered saline (PBS) at a 1:10 weight/volume ratio, using a motorized Teflon-glass dounce homogenizer [18]. Brain homogenates were prepared into convenient working aliquots and stored at –80 °C. Before immunoassays, total protein concentrations were determined using DC Assay (Bio-Rad, Hercules, CA, USA), and appropriate volumes of ice-cold PBS were added in order to equalize protein concentrations across samples.

Antibodies

All commercial and locally produced primary antibodies used in the present study are listed in Supplementary Table S1. Production and characterization of mouse monoclonal antibodies against syntaxin-1 (clones SP6 and SP7), SNAP-25 (SP12 and SP14), VAMP (SP10 and SP11), complexin-I (SP33), complexin-II (LP27) and synaptotagmin (MAb30 and MAb48) was described elsewhere [39–41]. Peroxidase- and Alexa-Fluor 488/555/647-conjugated secondary antibodies were from Jackson ImmunoResearch Laboratories (West Grove, PA, USA) or Molecular Probes (Eugene, OR, USA), respectively.

SNARE reconstitution assays

Recombinant SNARE and accessory proteins were purchased from diverse commercial suppliers. Relevant features of these synthetic constructs are listed in Supplementary Table S2. *In vitro* presynaptic complex reconstitution was achieved by sequentially adding the appropriate recombinant proteins (as indicated in the corresponding figures) into the reaction buffer (PBS with or without 1 mM Ca^{2+}) to a final concentration of 1 μM each. Mixtures were incubated at 37 °C for 30 min prior separation in native gels, as indicated below. Reconstituted protein complexes were either resolved by gel de-staining to remove excess of coomassie dye following manufacturer's instructions, or transferred to polyvinylidene difluoride (PVDF) membranes and finally immunoblotted with specific antibodies, as indicated below.

Immunoprecipitation

The native co-immunoprecipitation (IP) approach to extract and characterize SNARE and other presynaptic protein complexes was performed using sheep anti-mouse IgG-coated magnetic Dynabeads (Life Technologies, Carlsbad, CA, USA), as reported [29]. Briefly, human brain homogenetes were initially solubilized in PBS supplemented with 1% Triton X-100, and 1% of protease inhibitors (Sigma-Aldrich, St. Louis, MO, USA) for 1 h at 4 °C. Insoluble material was precipitated at 16,000 *g* for 30 min at 4 °C, and supernatants were incubated overnight with primary antibody-conjugated beads at 4 °C with gentle rotation. After thorough washing, a mild 10 mM Tricine buffer (pH 2.3) was added to the reactions to elute protein complexes from the beads while preserving protein-protein interactions. All IP reactions were run in triplicate along appropriate negative controls [29], and the IP products were finally resolved by native and/or standard electrophoresis.

Native and denaturing gel electrophoresis, and quantitative immunoassays

Quantitative one- (1-D) and qualitative two- (2-D) dimension blue-native (BN) and sodium-dodecyl sulfate (SDS) polyacrylamide electrophoreses (PAGE) were performed essentially as previously described [29], using either 4–16% gradient NativePAGE precast gels (Novex, Carlsbad, CA, USA) and/or 12% minigels (Bio-Rad), respectively. Solubilized human brain samples, IP products or recombinant protein mixtures were combined with equal volumes of native (0.5% Triton X-100, 0.25% Coomassie brilliant blue G-250, 10% glycerol) or denaturing (100 mM Tris, pH 6.8, 4% SDS, 0.2% bromophenol blue, 20% glycerol, 200 mM β-mercaptoethanol) buffers before loading into the gels. In quantitative experiments, standard samples were generated by pooling equal amounts from all IT or all MF human homogenates, and loaded in triplicate along the samples in all gels of the study [23]. Similarly, specific molecular size ladders for BN- or SDS-PAGE were also loaded into the gels to identify complexes and proteins. A total protein load of 5 μg, combined with multipoint imaging exposure times (20 s to 3 min), was found optimal to quantify all presynaptic complexes from brain homogenates within the linear range (see e.g. Supplementary Fig. S1). After electrophoresis, proteins were transferred to PVDF membranes, and subsequently blocked (1 h), and incubated with primary (overnight, 4°C; see Supplementary Table S1) and secondary (1 h; 1:5000) antibodies, in TBS containing 5% milk and 0.1% Tween-20. Chemiluminescence was enhanced with commercial reagents (Perkin Elmer, Waltham, MA, USA), and images were digitized using a LAS-3000 Image Reader (Fujifilm, Tokyo, Japan). Densitometric analyses of the immunoblots were done with ImageGauge software, version 4.22 (Fujifilm). Quality control measures were taken to maximize the accuracy and reproducibility of the quantitative studies, as previously documented [23,24]. The amounts of SNARE and other presynaptic proteins in MAP brain samples were immunoassayed in previous studies [18].

Immunofluorescence

Paraffin-embedded (6-μm-thick) and free-floating (40-μm-thick) human hippocampal sections were obtained from the above mentioned paraformaldehyde-fixed tissue blocks, from $n = 7$ MAP participants with mild-to-moderate AD, as previously described [24]. Triple immunostaining procedures were as reported [23,42]. We first evaluated the

distribution patterns in the different immunostained slices to ensure antibody specificity and proper labeling of the proteins targeted. To this end, images from the entire hippocampal formation were acquired from the paraffin-embedded slices using a Nikon Eclipse 80i microscope equipped with epifluorescence module, a motorized stage and a 10x/0.30NA objective (Nikon, Tokyo, Japan). For colocalization studies, the immunostained floating sections were imaged as reported [41] in a Zeiss confocal microscope equipped with a LSM 5 Pascal Module and a 63×/1.2NA water immersion objective (Zeiss, Jena, Germany). All appropriate positive and negative controls were included in every experimental run. Image processing for background subtraction, thresholding and colocalization analyses were performed in ImageJ 2.0 (NIH, Bethesda, MA, USA) using built-in, unbiased algorithms [41,43].

Statistical analyses

In quantitative immunoblotting assays, densities of the identified complexes were first calculated as a percentage of in-gel standards [29,44]. For some analyses, the ratio between the immunodensities of complexin-I to complexin-II equivalent complexes was used as an index of inhibitory/excitatory functional input [24,42]. Normal distribution of the data was confirmed with the Kolmogorov-Smirnov test. Initial multivariate analyses were performed to inspect associations between the amounts of proteins and complexes, and the multiple clinic-pathological and demographic features of MAP participants. Analysis of covariance (ANCOVA), adjusting for age, sex, education and postmortem interval (PMI), was used to detect differences between clinically and pathologically diagnosed groups, using Dunnett's *post hoc* test. The associations between cognitive function (outcome) and the multiple neurochemical measures of the study (predictors) were tested in multiple linear regression models covarying by demographic and pathologic variables. Additionally, all models were adjusted by the mean of the total immunodensities of the three SNARE proteins (syntaxin-1, SNAP25, VAMP), independently assessed in the same brain homogenates by ELISA. The purpose of the latter covarying approach is two-fold, housekeeping for variations in SNARE protein expression levels, and controlling for synapse density [24]. Alternatively, covarying by the total density of the specific protein targeted in each complex measure yielded very similar results (data not shown). Double dissociation models were used to demonstrate the separate contributions of different brain regions, via different neurochemical measures, to global cognitive function [45]. The associations between longitudinally ascertained cognitive decline (outcome) and the multiple variables of the study were also assessed. Linear mixed-effects models with random intercept and slope terms were used to examine individual participant trajectories of cognition over time. The fixed effects estimated the association between neurochemical measures and cognition over time, adjusting for covariates. The random intercept and slope terms accounted for within-subject correlation and between-subject variability. These models allowed for the intercept (cognition at time of death) and slope (rate of cognitive decline over time) to vary by subject. Additionally, a previous study with this cohort identified that the rate of cognitive decline changed 3.0 years (95% confidence interval 2.7 to 3.2 years) prior to death, delineating a period of terminal cognitive decline in the final years of life [7]. A second temporal term was added to the model to allow each individual trajectory to have a distinct slope during the preterminal and terminal periods of cognitive decline. A stepwise model specification process retained covariates that

improved model fit by comparing the Akaike Information Criterion (AIC) and deviance statistic values of nested models. Nested models were also compared by likelihood ratio test. For the final adjusted model, all possible interaction terms were tested to examine the relationship between neurochemical factors and rate of cognitive decline. The percent contribution of each neurochemical measure to reduce between-subject cognitive variance was defined as the difference between whole model adjusted R^2 values obtained in nested models with and without the term for the assessed protein complex. Standardized beta coefficients (β) are reported to compare the weight of each variable within a model. Whenever appropriate, p-values were adjusted for false discovery rate (FDR), and the level of significance was set to FDR $P < 0.05$. All datasets were analyzed and plotted with JMP (V.12.1; SAS Institute, Cary, NC, USA), R (V.3.0.3; R-project) [46], and/or Prism (V.6.0; GraphPad Software, La Jolla, CA, USA).

Results

Identification and characterization of brain presynaptic complexes in native gels

In previous studies documenting complexes formed by SNARE proteins in human and rodent brain homogenates [29], the oligomeric structures containing complexins-I/II were incompletely addressed. To expand the characterization of the native SNARE interactome, we adopted two different but complementary approaches: (1) reconstitution assays using purified recombinant proteins, and (2) multistep separation of solubilized brain complexes from cortical homogenates.

In crude brain homogenates separated by 1-D BN-PAGE, we identified multiple bands for all proteins immunolabeled, allowing quantification of some (but not all) of the resolved oligomers (Fig. 1a). The sizes of the protein complexes reported below are relative to the molecular markers loaded alongside in the gels, and are approximate measures. The complexes detected by labeling syntaxin-1 (at 450, 150 and 30 kDa), SNAP25 (at 450, 150 and 70 kDa), and VAMP (450, 150, 70 and 15 kDa; not shown) were comprehensively characterized previously with up to 9 different SNARE antibodies [29], and were consistently visualized in the present study (Fig. 1a). The bands detected at 150 and 450 kDa were the major, fully loaded SNARE complexes, while the 70-kDa complex was revealed as a SNAP25-VAMP heteromer [29]. In the present study, SNARE complexes were only quantified with antibodies against syntaxin-1 and SNAP25, as we failed to obtain consistent sharp bands when probing with anti-VAMP antibodies (see Supplementary Fig. S1). Both complexins displayed identical fingerprints in 1-D BN-gels, with a major complex at ~200 kDa, and other sharp bands at ~500 and ~50 kDa (Fig. 1a), indicating that complexin-I (mainly inhibitory) and complexin-II (mainly excitatory) containing presynaptic terminals can build similar SNARE machineries. Other bands were inconsistently observed, and therefore not quantified. Similarly, for all probed synaptic proteins, a gradient of heavy weight complexes (multimers) was also detected above 500 kDa.

In vitro reconstitution assays were performed to verify the composition of the observed bands in native immunoblots from human brain extractions. Mixtures containing equimolar amounts of the SNARE proteins recapitulated the two major SNARE bands observed in brain homogenates at 150 and 450 kDa, plus a third complex at 250 kDa inconsistently

observed in brain extracts (compare syntaxin-1 and SNAP25 immunoblots in Figs. 1A–C). Anti-VAMP antibodies were poorly immunoreactive with these complexes possibly related to steric hindrance under native conditions. Addition of recombinant munc18–1 did not modify the observed band sizes or densities, indicating that either the assay conditions are not suitable for munc18–1-syntaxin-1 interaction, or that munc18–1 dissociates from the complex during the electrophoretic separation. Importantly, following incorporation of recombinant complexin-I in the reactions, substantial changes were observed in band distribution patterns. Thus, in syntaxin-1 immunoblots, complexin-I seemed to combine with the 150- and 450-kDa SNARE complexes, as new (though diffuse) bands appeared at 200 and 500 kDa (Fig. 1b), while the 250-kDa syntaxin-1 complex completely vanished. Indeed, these 200- and 500-kDa bands were the major oligomers observed when labeling complexin-I (Fig. 1b), and resembled those observed in brain homogenates (Fig. 1a). Similar to munc18–1, addition of synaptotagmin (the Ca^{2+} sensor in SNARE-mediated neurosecretion), in the absence or presence of Ca^{2+}, had no significant effect on the observed complex sizes, although their immunodensities seemed mildly less.

In the second characterization approach we tested the functional interactions between these molecular complexes in human brain extracts by first immunoprecipitating with syntaxin-1, SNAP25, or complexin-I/II antibodies, and then separation by 1-D BN- (Fig. 1c) and 2-D SDS-PAGE (Fig. 1d), followed by immunoblotting. As previously shown [29], the 150 and 450-kDa SNARE complexes, but not the 70-kDa or the corresponding monomeric bands, were cross-detected in syntaxin-1 and SNAP25 IP products regardless of the SNARE protein immunolabeled. These complexes (including 70-kDa SNAP25) were also detected in complexin-II, and to a much lesser extent in complexin-I [24], IP products (Fig. 1c). Because of the longer exposure times required to reveal complexin-I/II probing bands, the antibody used in the IP reactions interfered with the specific signals from the immunoprecipitated complexes. Thus, we performed 2-D BN/SDS-PAGE allowing separation of the co-immunoprecipitated monomeric components, and confirmed that at least the 200-kDa complexin-I/II cross-reacts with SNARE proteins, and that a wide variety of SNARE complexes are precipitated by complexin antibodies (Fig. 1d).

In summary, these studies provided evidence supporting the interpretation that SNARE proteins and/or complexin-I/II are sufficient to build the complexes quantified in brain samples from MAP participants.

Descriptive statistics of MAP participants and potential confounds

Demographic, cognitive and pathological variables of MAP participants with available samples from the IT and/or the MF are summarized in Table 1. The characteristics of participants with available samples from both regions (i.e. overlap group; $n = 140$) were not significantly different from those of the whole group ($n = 188$), and therefore all available cases were used whenever possible to maximize the statistical power of the analyses. Within the whole group, 74 participants suffered from dementia, 55 displayed MCI, and 59 were cognitively healthy. The number of cases presenting macro- (32%) or microinfarcts (23%), Lewy bodies (19%), and hippocampal sclerosis (7%) were similar to other community

sample studies [7,33]. The age related pathologies (plaques and tangles) were present in almost all participants, although with wide variability in load and spread (Table 1).

Preliminary multivariate analyses were performed to inspect potential confounding factors, including (but not limited to) drug and alcohol consumption, depressive symptoms, comorbidities with other diseases, or *APOE* genotypes. Only PMI consistently showed significant associations with some of the neurochemical measures of the study, and therefore all statistical analyses used this potential confounder as a covariate.

Neurochemical, pathologic and cognitive correlates in MAP participants

In multivariate analyses, total protein amounts and complex immunodensities showed high correlations within and across brain regions (data not shown), suggesting the expression of these complexes is somewhat coordinated by upstream mechanisms. Pairwise correlations between the presynaptic proteins and complexes analyzed in the IT and MF, and some of the relevant pathologic, stereological and cognitive indices are summarized in Fig. 2.

Globally, as expected, greater densities of synaptic proteins and complexes were associated with lower burden of AD-related pathology as well as greater cognitive function nearest death. Particularly, tangle, rather than plaque, pathology showed stronger associations with synaptic complexes. These findings remained unchanged regardless of whether local (i.e. within region) or global brain (z-scores across regions) pathological measurements were used. In regard to non-AD neuropathologies, the severity of arteriolosclerosis correlated with higher amounts of syntaxin-1, SNAP25 and synaptophysin in MF, but not their corresponding complexes. The presence of other age-related pathologies did not seem to affect significantly the levels of the synaptic markers in the MAP participants studied.

Interestingly, greater numbers of either resting or activated microglial cells were associated with lower density of synaptic proteins. These associations were particularly strong for activated microglia in the IT, despite the number of these cells being slightly lower than in MF. Notably, larger microglial cell counts had no great impact on the amount of presynaptic PPIs, with the exception of heavy complexin-I MF complexes. These inverse associations may underlie microglial synaptic surveillance and “pruning” activities [47,48]. While this mechanism has been widely described in laboratory animals, few investigations are available for microglial-mediated synaptic phagocytosis in aging human brain [49,50]. We therefore performed series of colocalization studies in available hippocampal slices of MAP participants aimed at demonstrating overlap between synaptic material and HLA-DR positive microglia. As expected, antibodies against the presynaptic markers and anti-HLA-DR presumably labeled neuropil and microglial cells respectively (Fig. 3a). For all presynaptic proteins targeted (SNAP25, VAMP and complexin-1 are shown in Fig. 3b,c) significant colocalization was observed with HLA-DR positive microglia, using an unbiased analytical approach [43]. This was particularly evident in areas with neuritic pathology, as documented with either Alz-50 (Fig. 3c) or AT8 (not shown) antibodies, where abundant activated microglia were present. Similar results were obtained in all subjects analyzed (n = 7). Combined, the above observations suggest that microglial phagocytic activity may preferentially target dystrophic terminals with poor trafficking activity (i.e. low SNARE PPIs).

Among the presynaptic interactome in the IT, most of the SNARE and complexin-II (mainly glutamatergic) species were highly correlated with cognition, whereas in the MF, the associations with cognitive outcomes were particularly led by 70-kDa SNAP25 and complexin-I (mainly GABAergic) complexes. The ratios between the immunodensities of complexin-I to complexin-II equivalent complexes (200 and 500 kDa) in the MF were also strongly associated with cognitive scores, indicating a high sensitivity of cognition to inhibitory/excitatory imbalance. These neurochemical-cognitive correlations did not show a clear specificity for a particular cognitive domain, which in turn were consistent with MMSE data. These observations were in agreement with the correlations between the cognitive outcomes and overall SNARE PPIs assayed in parallel by “capture” ELISA. The notable associations between complexin-I/II total protein levels and cognition were documented previously [24].

The above findings were also consistent with the distribution of presynaptic complexes across the pathologically and clinically diagnosed groups. Thus, no significant differences were observed between CERAD-scaled participants (i.e. ranked according to the severity of plaque pathology) for any of the complexes in either brain area (Fig. 4a). In contrast, in the IT (but not MF) of participants at late Braak stage (i.e. widespread tauopathy), the levels of SNARE and complexin-II (200 and 500 kDa) complexes were significantly lower than in subjects at early stages (Fig. 4b). Likewise, multiple SNARE complexes and 200-kDa complexin-I and -II oligomers were downregulated in the IT of participants with dementia compared to those who were cognitively normal by the time of death (Fig. 4c). Yet, in the MF of participants with dementia, only 70-kDa SNAP25 and 500-kDa complexin-I were found altered.

Contributions of the SNARE protein interactome to cognitive function and decline

We conducted a series of models to study the associations between cognitive scores and the SNARE interactome, adjusting for demographics and covarying by cerebrovascular diseases, Lewy bodies, hippocampal sclerosis and local amyloid and tau pathologies (see Supplementary Table S3). Models were also controlled for the average of SNARE protein immunodensities to account for total protein synthesis at synapses and/or the synaptic density [24]. In FDR-adjusted models, most neurochemical-cognitive associations remained significant after controlling for relevant confounders and pathologies (Supplementary Table S3). Within the SNARE interactome measures, the most remarkable predictors of cognitive function were 150-kDa syntaxin-1 in the IT and the ratio between the 500-kDa species of complexins-I/II in the MF, contributing 8.6 and 9.6% to variance, respectively (FDR $P < 0.001$ in both cases) (Supplementary Table S3). Multiple modeling using different combinations of the quantified complexes within region determined that these two measures (i.e. IT 150-kDa syntaxin-1 and MF 500-kDa complexin-I/II ratio) mediated the effects on cognition of all other synaptic proteins and complexes (data not shown). Interestingly, combining these two major synaptic indices across brain regions, greater levels of each IT 150-kDa syntaxin-1 and MF 500-kDa complexin-I/II ratio were similarly associated with higher cognitive scores nearest death, with a combined contribution of 13% to the between-subject cognitive variance (comparing the Reference Model and Model 3 in Table 2), after adjusting for demographics and neuropathologies (FDR-$P = 0.0068$ each).

Notably, the above complexes were not associated with cognitive function nearest death when using data obtained in the alternative lobe (i.e. MF 150-kDa syntaxin-1 and IT complexin-I/II ratio), suggesting the existence of double dissociation between temporal lobe pan-synaptic functionality and frontal lobe GABAergic/glutamatergic function affecting cognition. This hypothesis was tested in a regression model where both neurochemical measures in IT and MF were crossed with a term for brain area as a within-subject factor, predicting cognition and covarying for demographic and neuropathologic variables. In this model, the interaction terms for both neurochemical measures were highly significant (Fig. 5a). In contrast, similar interaction terms between brain area and either amyloid-β load or phosphotau deposition were at best marginally significant (Fig. 5a), likely because both pathologic indices contributed to lower cognitive function regardless of the brain area in which they accumulated. Replacing amyloid-β and phosphotau immunohistochemical data for plaque and NFT counts did not change the above observations (data not shown).

The semi-additive nature of these synaptic measures in each brain region suggests that frontal and temporal synaptic dysfunctions occur in a relatively inter-independent manner, and might explain different cognitive mechanisms. To further explore this possibility, we replicated Model 3 in Table 2 replacing global cognitive scores by the scores testing the different cognitive domains, as well as the slopes calculated for longitudinal global cognitive decline, as outcomes in multiple linear regression models (see Supplementary Table S4). Thus, greater IT 150-kDa syntaxin-1 levels were associated with better semantic memory and visuospatial skills, whereas increased density of the 500-kDa complexin I/II ratio in MF was significantly associated with higher episodic memory and perceptual speed. Interestingly, lower amounts of both synaptic indices similarly contributed to faster rates of longitudinal cognitive decline.

To gain more insight into the influence of a possible collapse of the presynaptic interactome on the rate of cognitive decline in old age, we constructed linear mixed-effect models of change in global cognition over time in the years prior to death. Models were adjusted for demographic and pathologic covariates and included a change-point parameter delineating the terminal decline phase fixed at three years prior to death to estimate the effects of IT 150-kDa syntaxin-1 levels and MF 500-kDa complexin I/II ratio on the rate of preterminal and terminal cognitive decline. Overall, the final three years of life were associated with a 59% increase in rate of cognitive decline compared to the preterminal phase. As expected, greater SNARE interactome values predicted slower rates of cognitive decline (IT 150-kDa syntaxin-1: $\beta = 0.002 \pm 0.001$, $P < 0.001$; MF 500-kDa complexin I/II ratio: $\beta = 0.025 \pm 0.012$, $P = 0.032$) and higher global cognitive scores at end of life ($\beta = 0.015 \pm 0.004$, $P < 0.001$; and $\beta = 0.190 \pm 0.078$, $P = 0.015$, respectively) in MAP participants (Supplementary Table S5). For example, cognitive function of participants displaying postmortem values within the lower tertile of IT 150-kDa syntaxin-1 declined 2.44 times faster than those in the higher tertile of these synaptic indices (Fig. 5b). Likewise, individuals with the lowest tertile of the MF 500-kDa complexin I/II ratio experienced a rate of cognitive decline that was 1.49 times faster than those with the highest levels. The 150-kDa syntaxin-1 levels and 500-kDa complexin I/II ratio accounted for 7.5% and 1.0% of the variation in cognition over time, respectively (Supplementary Table S5). Conversely, amyloid-β load ($\beta = -0.033 \pm 0.009$, $P < 0.001$) and Lewy Body disease were associated with faster cognitive decline over time, with

the latter particularly affecting the rate of terminal decline in the final three years of life (β = 0.296±0.059, $P < 0.001$). These two neuropathologies explained 6.0% and 4.8% of the variance, respectively. Note that these models do not take into account variations in the synaptic (and other pathologic) indices accompanying cognitive decline prior to death, which should be recognized as a major limitation of this particular 'predictive' approach.

Finally, we addressed the question of whether these associations might occur at early or late stage of AD. In similar regression models, we introduced variables for Braak stage or CERAD scale, and crossed them with those of the presynaptic complex immunodensities. As graphically expressed for 150-kDa syntaxin-1 and 500-kDa complexin-I/II ratio at the different Braak stages (Supplementary Fig. S2), none of these interaction terms showed significant associations with cognition, and therefore stage-dependent effects were discarded. Furthermore, the above neurochemical-cognitive associations did not occur in interaction with the different age-related pathologies, as the added interaction terms between complex immunodensities and the pathologic indices were not significant predictors of cognitive function nearest death (data not shown).

Discussion

We investigated the complex associations between cognitive function, age-related neuropathology, and the SNARE interactome (as an index of synaptic functionality) in a well-characterized, community-dwelling population. The results indicate that SNARE interactome dysregulation may occur independent from co-occurring pathologic insults, and is in turn strongly associated with cognitive impairment in the elderly. The particular cognitive domains sensitive to this type of synaptic dysfunction differed according to the brain area affected. Thus, pan-synaptic disruption in the temporal lobe was particularly associated with semantic memory and visuospatial skills deficits, while the inhibitory/excitatory imbalance in frontal lobe was associated with episodic memory and perceptual speed. Given its strong association with higher rates of cognitive decline, disruption of the SNARE interactome might be an early event in the expression of brain aging.

Although research on the neurobiology of vesicle trafficking experienced an exponential growth in the past decades, the complete sequence of SNARE interactome consolidation, and the precise function(s) of each SNARE modulator are still unclear [20,51]. In the presynaptic terminals, under low Ca^{2+} concentration conditions, the monomeric components of SNARE machinery bind with weak interactions, forming multiple preassembled structures of variable conformation and stoichiometry, which dock vesicles to the presynaptic membrane (see schematic cartoon in Fig. 6). Priming may occur following the incorporation of new SNARE partners to the complex, while strengthening SNARE associations. While synaptotagmin acts as a Ca^{2+} sensor [52], the role of complexins is less clear, and may include anchoring synaptotagmin into the complex, or possibly clamping the complex to prevent unnecessary firing events in the absence of Ca^{2+} [53–55].

The minimal number of SNARE complexes required to successfully prime a synaptic vesicle and open a fusion pore is also a matter of debate. *In vitro* experiments demonstrated that one single SNARE heterotrimer could be sufficient to complete a fusion event [56], although a

greater number of complexes are thought to be required under physiological conditions [57–59]. While the present reconstitution assays were not originally conceived to resolve any of the above questions, our findings in non-denaturing gels may additionally provide direct evidence supporting that the SNARE heterotrimeric complexes associate by pairs. Thus, the smallest and most abundant SNARE species was observed at ~150 kDa, compatible with a dimer of heterotrimers (note that the theoretical molecular mass for each syntaxin-1+SNAP25+VAMP complex is ~72 kDa). In turn, the ~450-kDa complex, also reconstituted by the three isolated SNARE proteins, could fit with a hexameric stoichiometry of heterotrimers. The addition of complexin-1 to the reactions resulted in the constitution of ~200 and ~500-kDa complexes, which might also be compatible with the above dimeric and hexameric stoichiometries of SNARE+complexin heteromers. The present assay, however, failed to resolve complexes containing munc18–1 or synaptotagmin, which are essential contributors to the SNARE interactome, and Ca^{2+} addition did not modify these properties. Likely, the reconstituted heteromeric structures may correspond to preassembled complexes prior to vesicle fusion. In contrast, the 70-kDa complex, at least containing SNAP25 and VAMP [29], also unobserved in the reconstitution assays, might be a consequence of SNARE recycling following fusion events [20]. Despite the above limitations, a simplified model is suggested in Fig. 6, depicting the different SNARE species observed *in vitro* and *in vivo* in a sequence of intermediate structures driving presynaptic vesicles through the docking, priming and fusion steps. The model assumes that a greater number of molecules attached to the SNARE machinery results in stronger priming of the vesicle, increasing the likelihood of fusion. Overall, our *in vitro* studies demonstrated that certain properties of the observed complexes in postmortem brain tissue could be mimicked by purified recombinant proteins. These data, however, need careful interpretation as the complexes (and stoichiometries) immunodetected in solubilized tissues and in reconstitution assays *in vitro* may vary in a cellular environment. Moreover, since some of the SNARE components were barely (i.e. VAMP) or not (e.g. Munc18–1) observed, definitive studies of the composition of those complexes likely require in-gel digestion followed by mass spectrometry. Unfortunately, all our efforts developing an assay to extract these synaptic complexes out of the native gels and further proteomic analyses were frustrated, perhaps due to the low efficiency of the extraction procedure.

Importantly, cortical immunodensities of multiple presynaptic complexes were strongly associated with the antemortem cognitive function of MAP participants. Because BN-PAGE experiments were performed with solubilized homogenates where protein-protein interactions remain dynamic [29], the resulting data may not simply illustrate the number of complexes proximate to death, but could reflect the functionality of the presynaptic interactome, understood as the capacity for producing fusion events upon demand. In the temporal lobe, the SNARE complexes showing the strongest association with cognition were those labeled with anti-syntaxin-1 antibody (particularly the 150-kDa complex), most likely representing the pan-synaptic interactome. While the immunodetected complexes using either anti-syntaxin-1 or anti-SNAP25 antibodies presumably correspond to the same presynaptic structures, substantial variability was observed on their separate associations with cognitive function, especially for the 450-kDa SNAREs in the IT. At least part of this variability might be attributed to the physiologically occurring SNAP25 self-aggregation,

demonstrated in reconstitution assays *in vitro*. This SNAP25 property may distort the quantitative data when comparing the results obtained in syntaxin-1 *versus* SNAP25 immunoblots. In contrast to the IT, in the MF, only complexin-I complexes (mainly present in inhibitory terminals), and more significantly the complexin-I/II ratio (i.e. inhibitory/excitatory input) had greater impact on the overall cognitive performance. It should be noted that no canonical GABA/glutamatergic markers were analyzed in the present study, and the assumptions of inhibitory/excitatory specificity are based on the pronounced segregation of complexins I and II between GABAergic and glutamatergic terminals, respectively [24,42]. Remarkably, the above associations were relatively independent from the global burden of neuropathology, and were also controlled for the total SNARE protein content as an index of overall synapse density. The cognitive domains associated with temporal pan-synaptic (semantic memory and visuospatial skills) and frontal inhibitory (episodic memory and perceptual speed) synaptic dysregulation also differed, suggesting that presynaptic interactome pathology may also define dementia types.

Consistent with our findings in MF, in previous studies analyzing a larger postmortem sample collection, we highlighted the greater impact of GABAergic synapse loss on cognitive performance in subjects at early Braak stages, which indicated that failure of the inhibitory system may trigger the cascade of events leading to cognitive decline [23,24]. These observations are in agreement with other clinical and preclinical studies implicating the inhibitory system in early cognitive impairment in the elderly [60–63], and advocate for a GABAergic-based therapy in AD [64,65]. Likewise, our data also support prior studies reporting enhanced cognitive performance in elderly patients with diverse pathologies treated with the antiepileptic drug levitracetam [66,67], a compound known to target the presynaptic machinery via synaptic vesicle-2A protein [68,69]. Additionally, in both brain areas, the 70-kDa SNAP25 species were significantly associated with cognitive function. According to the model hypothesized in Fig. 6, this latter observation might indicate that dysregulation of the presynaptic machinery could be triggered by dysfunctional SNARE protein recycling mechanisms [29].

Longitudinal models identified independent effects of 150-kDa syntaxin-1 levels in IT and the MF 500-kDa complexin I/II ratio on the rate of cognitive decline in the final years of life. Thus, lower levels of each of these presynaptic indices were associated with faster decline rates, adjusting for other neurochemical and demographic factors. Early loss of frontotemporal connectivity may contribute meaningfully to the rate of cognitive decline in at least the last decade of life. Notably, the SNARE interactome deficits affected cognitive performance regardless of the accumulation of multiple neuropathologies, suggesting that AD pathology is not responsible for the above synaptic deficits.

Although the present study mainly focused on the contributions of synaptic deficits and the pathologic indices to cognitive function in MAP participants as relatively separate entities, previous and present results also indicated the existence of crosstalk mechanisms between synaptopathy and other brain pathologies. Thus, AD-related pathologies showed complex, and region-dependent associations with the synaptic targets of the study. Similar to their associations with cognitive outcomes, IT presynaptic complexes correlated with tangle and neuritic pathology, whereas the GABAergic interactome (i.e. complexin-I PPIs) was the

strongest predictor of MF tauopathy. Whether or not any of these associations are causal is difficult to determine. While the deleterious effect of AD pathology on nerve endings is widely accepted [10], others have reported accelerated phosphotau spread associated with enhanced glutamatergic excitability [70]. As remarkable as unexpected was the association between SNARE protein levels and the severity of arteriolosclerosis. This association, especially significant in MF, has not been described earlier and therefore deserves more attention in future studies. A previous report suggested that arteriolosclerosis could cause axonal lesions interrupting axonal transport and the concomitant accumulation of presynaptic material, including synaptophysin [71]. Of note, other cerebrovascular diseases, such as macro- and microinfarcts, did not show such strong correlations with the SNARE proteins, possibly suggesting a certain degree of specificity for the arteriolosclerosis findings. Notably, the presence of Lewy bodies greatly contributed to lower cognitive function in the current MAP cohort. Indeed, animal models of dementia with Lewy bodies overexpressing α-synuclein (the main component in these brain lesions) demonstrated the causative association between synucleinopathies and cognitive decline [72]. Recently, a physiological role for α-synuclein in SNARE-mediated exocytosis was described [73]. Despite the strong impact of Lewy bodies in MAP participants' cognitive abilities and the relevant synaptic function of α-synuclein, we did not observe significant associations between presynaptic protein levels and Lewy body disease. Further research will be needed to understand the pathologic mechanisms of linking presynaptic proteins and α-synuclein. Finally, microglial pruning activity did not appear to explain the SNARE interactome dysfunction in MAP participants. While strong and inverse correlations were observed between the total amounts of presynaptic protein and activated microglial cell densities, the associations between the counts of these phagocytic cells and SNARE PPIs were not evident. Although speculative, microglial pruning activity could be selectively directed to dysfunctional synapses with poor neurotransmitter release activity (i.e. less SNARE complex formation), obscuring an association with overall SNARE PPIs. Complexin-I high magnitude complexes seemed especially sensitive to microglial activation, which may suggest a preferential affinity of these cells for pruning active inhibitory over excitatory synapses. Future studies will explore whether this potential preference might be related to the inhibitory/excitatory imbalance reported in the present MAP sample.

Conclusions

The capability of the presynaptic machinery to remain functional across lifespan might be a fundamental source of brain reserve, as loss of SNARE functionality profoundly influences cognitive performance in the elderly. These observations were relatively independent from age-related neuropathology accumulation and synapse loss. Pharmacological strategies enhancing SNARE function, particularly at inhibitory synapses, might be fruitful to prevent or minimize cognitive deterioration in old age.

Supplementary Material

Refer to Web version on PubMed Central for supplementary material.

Acknowledgements

The study was supported by the Canadian Institutes of Health Research (MT-14037, MOP-81112, to WGH), and the Jack Bell Chair in Schizophrenia. The Memory and Aging Project is a collaborative, multidisciplinary and translational research project subsidized by the National Institute on Aging (Grants R01AG17917 to DAB, and R01AG42210 to JAS). We wish to express our gratitude to all participants in MAP, and to the staff in Rush AD Center. We also thank Hong-Ying Li and Jenny Yang for their skillful technical assistance, and Dr. Peter Davies for providing the Alz-50 antibody.

Abbreviations:

1-D	one-dimension
2-D	two-dimension
AD	Alzheimer's disease
ANCOVA	analysis of covariance
APP	amyloid precursor protein
BA	Brodmann's area
BN-PAGE	blue native-PAGE
BSA	bovine serum albumin
Ca^{2+}	inorganic calcium ion
CERAD	Consortium to Establish a Registry for AD
CPLX	complexin
DC	detergent compatible
EDTA	ethylenediaminetetraacetic acid
ELISA	enzyme-linked immunoadsorbant assay
FDR	false discovery rate
GABA	gamma-aminobutyric acid
HLA-DR	human leukocyte antigen - antigen D-related
IP	immunoprecipitation
IT	inferior temporal gyrus
M18	munc18–1
MAP	Memory and Aging Project
MCI	mild cognitive impairment
MF	middle-frontal gyrus

MMSE	mini-mental score examination, NCI, no cognitive impairment
NFTs	neurofibrillary tangles
NIA	National Institute on Aging
PAGE	polyacrylamide gel electrophoresis
PBS	phosphate-buffered saline
PMI	postmortem interval
PPIs	protein-protein interactions
PVDF	polyvinylidene difluoride
SDS	sodium dodecyl sulfate
SNAP25	synaptosome-associated protein 25
SNARE	soluble *N*-ethylmaleimide-sensitive factor attachment protein receptor
STX1	syntaxin-1
TBS	Tris-buffered saline
VAMP	vesicle-associated membrane protein
WT	wild-type

References

1. Ernst RL, Hay JW. The US economic and social costs of Alzheimer's disease revisited. Am. J. Public Health 1994;84:1261–4. [PubMed: 8059882]
2. Aguero-Torres H, von Strauss E, Viitanen M, Winblad B, Fratiglioni L. Institutionalization in the elderly: the role of chronic diseases and dementia. Cross-sectional and longitudinal data from a population-based study. J. Clin. Epidemiol 2001;54:795–801. [PubMed: 11470388]
3. Snowden MB, Steinman LE, Bryant LL, Cherrier MM, Greenlund KJ, Leith KH, et al. Dementia and co-occurring chronic conditions: a systematic literature review to identify what is known and where are the gaps in the evidence? Int. J. Geriatr. Psychiatry 2017;32:357–71. [PubMed: 28146334]
4. Suthers K, Kim JK, Crimmins E. Life expectancy with cognitive impairment in the older population of the United States. J. Gerontol. B. Psychol. Sci. Soc. Sci 2003;58:S179–86. [PubMed: 12730319]
5. Kapasi A, DeCarli C, Schneider JA. Impact of multiple pathologies on the threshold for clinically overt dementia. Acta Neuropathol. 2017;134:171–86. [PubMed: 28488154]
6. Riley KP, Snowdon DA, Markesbery WR. Alzheimer's neurofibrillary pathology and the spectrum of cognitive function: Findings from the Nun Study. Ann. Neurol 2002;51:567–77. [PubMed: 12112102]
7. Boyle PA, Wilson RS, Yu L, Barr AM, Honer WG, Schneider JA, et al. Much of late life cognitive decline is not due to common neurodegenerative pathologies. Ann. Neurol 2013;74:478–89. [PubMed: 23798485]
8. Bryne C, Matthews FE, Xuereb JH, Broome JC, McKenzie J, Rossi M, et al. Pathological correlates of late-onset dementia in a multicentre, community-based population in England and Wales. Lancet. 2001;357:169–75. [PubMed: 11213093]

9. Snowdon DA, Greiner LH, Mortimer JA, Riley KP, Greiner PA, Markesbery WR. Brain Infarction and the Clinical Expression of Alzheimer Disease: The Nun Study. JAMA J. Am. Med. Assoc 1997;277:813–7.
10. Spires-Jones TL, Hyman BT. The Intersection of Amyloid Beta and Tau at Synapses in Alzheimer's Disease. Neuron. 2014;82:756–71. [PubMed: 24853936]
11. Scheibel ME, Lindsay RD, Tomiyasu U, Scheibel AB. Progressive dendritic changes in aging human cortex. Exp. Neurol 1975;47:392–403. [PubMed: 48474]
12. Honer WG, Dickson DW, Gleeson J, Davies P. Regional synaptic pathology in Alzheimer's disease. Neurobiol. Aging 1992;13:375–82. [PubMed: 1625766]
13. Dickson DW, Crystal HA, Bevona C, Honer W, Vincent I, Davies P. Correlations of synaptic and pathological markers with cognition of the elderly. Neurobiol. Aging 1995;16:285–98. [PubMed: 7566338]
14. Bereczki E, Francis PT, Howlett D, Pereira JB, Hoglund K, Bogstedt A, et al. Synaptic proteins predict cognitive decline in Alzheimer's disease and Lewy body dementia. Alzheimers. Dement 2016;12:1149–58. [PubMed: 27224930]
15. Bereczki E, Branca RM, Francis PT, Pereira JB, Baek J-H, Hortobagyi T, et al. Synaptic markers of cognitive decline in neurodegenerative diseases: a proteomic approach. Brain. 2018;
16. Masliah E, Terry RD, DeTeresa RM, Hansen LA. Immunohistochemical quantification of the synapse-related protein synaptophysin in Alzheimer disease. Neurosci. Lett 1989;103:234–9. [PubMed: 2505201]
17. Hamos JE, DeGennaro LJ, Drachman DA. Synaptic loss in Alzheimer's disease and other dementias. Neurology. 1989;39:355–355. [PubMed: 2927643]
18. Honer WG, Barr AM, Sawada K, Thornton AE, Morris MC, Leurgans SE, et al. Cognitive reserve, presynaptic proteins and dementia in the elderly. Transl. Psychiatry 2012;2:e114. [PubMed: 22832958]
19. Minger SL, Honer WG, Esiri MM, McDonald B, Keene J, Nicoll JA, et al. Synaptic pathology in prefrontal cortex is present only with severe dementia in Alzheimer disease. J. Neuropathol. Exp. Neurol 2001;60:929–36. [PubMed: 11589423]
20. Sudhof TC. Neurotransmitter release: the last millisecond in the life of a synaptic vesicle. Neuron. 2013;80:675–90. [PubMed: 24183019]
21. Sudhof TC, Rothman JE. Membrane fusion: grappling with SNARE and SM proteins. Science. 2009;323:474–7. [PubMed: 19164740]
22. Ramos-Miguel A, Barr AM, Honer WG. Spines, synapses, and schizophrenia. Biol. Psychiatry 2015;78:741–3. [PubMed: 26542741]
23. Ramos-Miguel A, Hercher C, Beasley CL, Barr AM, Bayer TA, Falkai P, et al. Loss of Munc18–1 long splice variant in GABAergic terminals is associated with cognitive decline and increased risk of dementia in a community sample. Mol. Neurodegener 2015;10:65. [PubMed: 26628003]
24. Ramos-Miguel A, Sawada K, Jones AA, Thornton AE, Barr AM, Leurgans SE, et al. Presynaptic proteins complexin-I and complexin-II differentially influence cognitive function in early and late stages of Alzheimer's disease. Acta Neuropathol. 2017;133:395–407. [PubMed: 27866231]
25. White CC, Yang H-S, Yu L, Chibnik LB, Dawe RJ, Yang J, et al. Identification of genes associated with dissociation of cognitive performance and neuropathological burden: Multistep analysis of genetic, epigenetic, and transcriptional data. PLoS Med. 2017;14:e1002287. [PubMed: 28441426]
26. Kim D, Ackerman SL. The UNC5C Netrin Receptor Regulates Dorsal Guidance of Mouse Hindbrain Axons. J. Neurosci 2011;31:2167–79. [PubMed: 21307253]
27. Bennett DA, Schneider JA, Buchman AS, Barnes LL, Boyle PA, Wilson RS. Overview and findings from the Rush Memory and Aging Project. Curr. Alzheimer Res 2012;9:646–63. [PubMed: 22471867]
28. Wittig I, Braun H-P, Schagger H. Blue native PAGE. Nat. Protoc 2006;1:418–28. [PubMed: 17406264]
29. Ramos-Miguel A, Beasley CL, Dwork AJ, Mann JJ, Rosoklija G, Barr AM, et al. Increased SNARE Protein-Protein Interactions in Orbitofrontal and Anterior Cingulate Cortices in Schizophrenia. Biol. Psychiatry 2015;78:361–73. [PubMed: 25662103]

30. Bennett DA, Schneider JA, Buchman AS, De Leon CM, Bienias JL, Wilson RS. The Rush Memory and Aging Project: Study design and baseline characteristics of the study cohort. Neuroepidemiology. 2005;25:163–75. [PubMed: 16103727]
31. McKhann G, Drachman D, Folstein M, Katzman R, Price D, Stadlan EM. Clinical diagnosis of Alzheimer's disease: Report of the NINCDS-ADRDA Work Group under the auspices of Department of Health and Human Services Task Force on Alzheimer's Disease. Neurology. 1984;34:939–939. [PubMed: 6610841]
32. Schneider JA, Wilson RS, Bienias JL, Evans DA, Bennett DA. Cerebral infarctions and the likelihood of dementia from Alzheimer disease pathology. Neurology. 2004;62:1148–55. [PubMed: 15079015]
33. Schneider JA, Arvanitakis Z, Bang W, Bennett DA. Mixed brain pathologies account for most dementia cases in community-dwelling older persons. Neurology. 2007;69:2197–204. [PubMed: 17568013]
34. Braak H, Braak E. Neuropathological stageing of Alzheimer-related changes. Acta Neuropathol. 1991;82:239–59. [PubMed: 1759558]
35. Newell KL, Hyman BT, Growdon JH, Hedley-Whyte ET. Application of the National Institute on Aging (NIA)-Reagan Institute criteria for the neuropathological diagnosis of Alzheimer disease. J. Neuropathol. Exp. Neurol 1999;58:1147–55. [PubMed: 10560657]
36. Mirra SS, Hart MN, Terry RD. Making the diagnosis of Alzheimer's disease: A primer for practicing pathologists. Arch. Pathol. Lab. Med 1993;117:132–44. [PubMed: 8427562]
37. Bradshaw EM, Chibnik LB, Keenan BT, Ottoboni L, Raj T, Tang A, et al. CD33 Alzheimer's disease locus: Altered monocyte function and amyloid biology. Nat. Neurosci 2013;16:848–50. [PubMed: 23708142]
38. Morrison JH, Baxter MG. The ageing cortical synapse: Hallmarks and implications for cognitive decline. Nat. Rev. Neurosci 2012;13:240–50. [PubMed: 22395804]
39. Barakauskas VE, Beasley CL, Barr AM, Ypsilanti AR, Li H-Y, Thornton AE, et al. A novel mechanism and treatment target for presynaptic abnormalities in specific striatal regions in schizophrenia. Neuropsychopharmacology. 2010;35:1226–38. [PubMed: 20072114]
40. Honer WG, Hu L, Davies P. Human synaptic proteins with a heterogeneous distribution in cerebellum and visual cortex. Brain Res. 1993;609:9–20. [PubMed: 7685234]
41. Ramos-Miguel A, Honer WG, Boyda HN, Sawada K, Beasley CL, Procyshyn RM, et al. Exercise prevents downregulation of hippocampal presynaptic proteins following olanzapine-elicited metabolic dysregulation in rats: Distinct roles of inhibitory and excitatory terminals. Neuroscience. 2015;301:298–311. [PubMed: 26086543]
42. Sawada K, Barr AM, Nakamura M, Arima K, Young CE, Dwork AJ, et al. Hippocampal complexin proteins and cognitive dysfunction in schizophrenia. Arch. Gen. Psychiatry 2005;62:263–72. [PubMed: 15753239]
43. Costes SV, Daelemans D, Dobbin Z, surname>Lockett S Automatic and quantitative measurement of protein-protein colocalization in live cells. Biophys. J 2004;86:3993–4003. [PubMed: 15189895]
44. Gil-Pisa I, Munarriz-Cuezva E, Ramos-Miguel A, Uriguen L, Meana JJ, Garcia-Sevilla JA. Regulation of munc18–1 and syntaxin-1A interactive partners in schizophrenia prefrontal cortex: down-regulation of munc18–1a isoform and 75 kDa SNARE complex after antipsychotic treatment. Int. J. Neuropsychopharmacol 2012;15:573–88. [PubMed: 21669024]
45. Van Orden GC, Pennington BF, Stone GO. What do double dissociations prove? Cogn. Sci 2001;25:111–72.
46. R Core Team. R: a language and environment for statistical computing. Vienna, Austria; 2015 2015.
47. Wake H, Moorhouse AJ, Jinno S, Kohsaka S, Nabekura J. Resting Microglia Directly Monitor the Functional State of Synapses In Vivo and Determine the Fate of Ischemic Terminals. J. Neurosci 2009;29:3974–80. [PubMed: 19339593]
48. Paolicelli RC, Bolasco G, Pagani F, Maggi L, Scianni M, Panzanelli P, et al. Synaptic pruning by microglia is necessary for normal brain development. Science. 2011;333:1456–8. [PubMed: 21778362]

49. Derecki NC, Katzmarski N, Kipnis J, Meyer-Luehmann M. Microglia as a critical player in both developmental and late-life CNS pathologies. Acta Neuropathol. 2014;128:333–45. [PubMed: 25056803]
50. Spangenberg EE, Green KN. Inflammation in Alzheimer's disease: Lessons learned from microglia-depletion models. Brain. Behav. Immun 2017;61:1–11. [PubMed: 27395435]
51. Jahn R, Fasshauer D. Molecular machines governing exocytosis of synaptic vesicles. Nature. 2012;490:201–7. [PubMed: 23060190]
52. Brose N, Petrenko A, Sudhof T, Jahn R. Synaptotagmin: a calcium sensor on the synaptic vesicle surface. Science. 1992;256:1021–5. [PubMed: 1589771]
53. Tang J, Maximov A, Shin OH, Dai H, Rizo J, Südhof TC. A Complexin/Synaptotagmin 1 Switch Controls Fast Synaptic Vesicle Exocytosis. Cell. 2006;126:1175–87. [PubMed: 16990140]
54. Melia TJ. Putting the clamps on membrane fusion: How complexin sets the stage for calcium-mediated exocytosis. FEBS Lett. 2007;581:2131–9. [PubMed: 17350005]
55. Trimbuch T, Rosenmund C. Should I stop or should I go? The role of complexin in neurotransmitter release. Nat. Rev. Neurosci. 2016;17:118–25.
56. Van Den Bogaart G, Holt MG, Bunt G, Riedel D, Wouters FS, Jahn R. One SNARE complex is sufficient for membrane fusion. Nat. Struct. Mol. Biol 2010;17:358–64. [PubMed: 20139985]
57. Mohrmann R, De Wit H, Verhage M, Neher E, Sørensen JB. Fast vesicle fusion in living cells requires at least three SNARE complexes. Science. 2010;330:502–5. [PubMed: 20847232]
58. Han X, Wang CT, Bai J, Chapman ER, Jackson MB. Transmembrane Segments of Syntaxin Line the Fusion Pore of Ca 2+-Triggered Exocytosis. Science. 2004;304:289–92. [PubMed: 15016962]
59. Shi L, Shen QT, Kiel A, Wang J, Wang HW, Melia TJ, et al. SNARE proteins: One to fuse and three to keep the nascent fusion pore open. Science. 2012;335:1355–9. [PubMed: 22422984]
60. Bakker A, Krauss GL, Albert MS, Speck CL, Jones LR, Stark CE, et al. Reduction of Hippocampal Hyperactivity Improves Cognition in Amnestic Mild Cognitive Impairment. Neuron. 2012;74:467–74. [PubMed: 22578498]
61. Koliatsos VE, Kecojevic A, Troncoso JC, Gastard MC, Bennett DA, Schneider JA. Early involvement of small inhibitory cortical interneurons in Alzheimer's disease. Acta Neuropathol. 2006;112:147–62. [PubMed: 16758165]
62. Li Y, Sun H, Chen Z, Xu H, Bu G, Zheng H. Implications of GABAergic neurotransmission in Alzheimer's disease. Front. Aging Neurosci 2016;8. [PubMed: 26858639]
63. Saura CA, Parra-Damas A, Enriquez-Barreto L. Gene expression parallels synaptic excitability and plasticity changes in Alzheimer's disease. Front. Cell. Neurosci 2015;9. [PubMed: 25698924]
64. Tong LM, Yoon SY, Andrews-Zwilling Y, Yang A, Lin V, Lei H, et al. Enhancing GABA Signaling during Middle Adulthood Prevents Age-Dependent GABAergic Interneuron Decline and Learning and Memory Deficits in ApoE4 Mice. J. Neurosci 2016;36:2316–22. [PubMed: 26888940]
65. Luo J, Lee SH, VandeVrede L, Qin Z, Piyankarage S, Tavassoli E, et al. Re-engineering a neuroprotective, clinical drug as a procognitive agent with high in vivo potency and with GABAA potentiating activity for use in dementia. BMC Neurosci. 2015;16:67. [PubMed: 26480871]
66. Cumbo E, Ligori LD. Levetiracetam, lamotrigine, and phenobarbital in patients with epileptic seizures and Alzheimer's disease. Epilepsy Behav. 2010;17:461–6. [PubMed: 20188634]
67. Sanchez PE, Zhu L, Verret L, Vossel KA, Orr AG, Cirrito JR, et al. Levetiracetam suppresses neuronal network dysfunction and reverses synaptic and cognitive deficits in an Alzheimer's disease model. Proc. Natl. Acad. Sci. U. S. A 2012;109:E2895–903. [PubMed: 22869752]
68. Matveeva EA, Vanaman TC, Whiteheart SW, Slevin JT. Levetiracetam prevents kindling-induced asymmetric accumulation of hippocampal 7S SNARE complexes. Epilepsia. 2008;49:1749–58. [PubMed: 18513349]
69. Lynch BA, Lambeng N, Nocka K, Kensel-Hammes P, Bajjalieh SM, Matagne A, et al. The synaptic vesicle protein SV2A is the binding site for the antiepileptic drug levetiracetam. Proc. Natl. Acad. Sci 2004;101:9861–6. [PubMed: 15210974]
70. Wu JW, Hussaini SA, Bastille IM, Rodriguez GA, Mrejeru A, Rilett K, et al. Neuronal activity enhances tau propagation and tau pathology in vivo. Nat. Neurosci 2016;19:1085–92. [PubMed: 27322420]

71. Suenaga T, Ohnishi K, Nishimura M, Nakamura S, Akiguchi I, Kumura J. Bundles of amyloid precursor protein-immunoreactive axons in human cerebrovascular white matter lesions. Acta Neuropathol. 1994;87:450–5. [PubMed: 8059597]

72. Hatami A, Chesselet MF. Transgenic rodent models to study alpha-synuclein pathogenesis, with a focus on cognitive deficits. Curr. Top. Behav. Neurosci 2015;22:303–30. [PubMed: 25218491]

73. Burré J, Sharma M, Tsetsenis T, Buchman V, Etherton MR, Südhof TC. Alpha-synuclein promotes SNARE-complex assembly in vivo and in vitro. Science. 2010;329:1663–7. [PubMed: 20798282]

Highlights

- Antemortem cognitive function is associated with postmortem SNARE interactome
- A poor SNARE interactome predicts faster rates of age-related cognitive decline
- SNARE protein levels, but not the interactome, are sensitive to microglial activation
- SNARE interactome dysfunction does not appear secondary to AD-related pathology

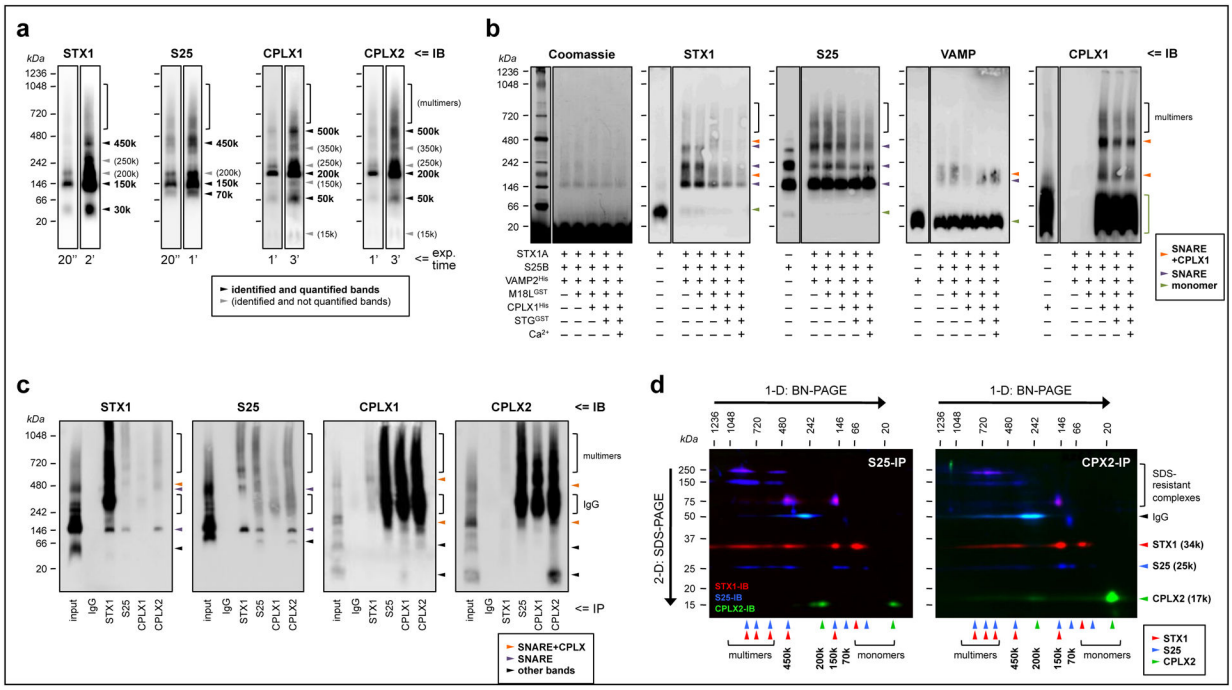

Fig. 1.

Characterization of the presynaptic complexes targeted in the present study. (**a**) Solubilized brain protein complexes from human inferior temporal cortex (IT) were resolved by blue-native (BN)-PAGE and immunoblotted (IB) with specific antibodies against syntaxin-1 (STX1), SNAP25 (S25) and complexins I (CPLX1) and II (CPLX2) (see Supplementary Table S1). The same representative case is shown in all individual immunoblots, with two exposure (exp.) times (ranging 20 s to 3 min; indicated at the bottom) per probing antibody. Arrowheads point to the identified and/or quantified complexes for each antibody. (**b**) Reconstitution assays were achieved by sequentially adding, from top to bottom, 1 μm of the recombinant proteins indicated (+) beneath the immunoblots. Abbreviations of the recombinant protein names and tags, and other key information of these constructs, are indicated in Supplementary Table S2. After incubation at 37°C for 30 min, the resulting protein complexes were resolved by BN-PAGE followed by Coomassie de-staining (following manufacturer's instructions), or immunolabeled as above. Antibodies against munc18–1 (long variant; M18L) and synaptotagmin (STG) were unable to react against their corresponding recombinant constructs under the present experimental conditions (not shown). Arrowheads point to the identified SNARE (purple) or SNARE+complexin (tangerine) heteromers, or the monomeric species (green) for each immunoblot. Of note, recombinant SNAP25 alone, but not syntaxin-1 or VAMP, mimicked all of the above bands, suggesting that SNAP25 has the ability to self-assemble into aggregates with similar stoichiometries as those in SNARE heteromers *in vitro* and *ex vivo*. While this observation represents a novel finding with potential implications for the biochemistry of SNARE dynamics, it is also beyond the aim and scope of the present work, and future studies should determine the physiological relevance (if any) of SNAP25 aggregates. (**c**) Human IT solubilized complexes were immunoprecipitated (IP) with anti-mouse IgG (negative control), anti-STX1, anti-SNAP25, anti-CPLX1, or anti-CPLX2 specific antibodies, and the

resulting IP products resolved, along the IP input sample, by BN-PAGE followed by immunoblotting standard procedures. (**d**) Anti-SNAP25 (left panel) and anti-CPLX2 (right panel) IP products were resolved by one- (1-D) followed by two-dimensional (2-D) BN +SDS-PAGE. Proteins were transferred to PVDF membranes and sequentially immunoblotted with anti-STX1 (red), anti-SNAP25 (blue), and anti-CPLX2 (green) specific antibodies. Top and left arrows indicate the directions of BN- and SDS-PAGE, respectively. Note the presence of SDS-resistant STX1/SNAP25 complexes/aggregates at 75–250 kDa, as well as the immunostaining for the primary antibodies used in IP at 50 kDa. For unknown reasons, the antibody-antigen reaction between the anti-SNAP25 antibody (i.e. SP12) used in the co-IP reactions and the anti-mouse IgG1 secondary antibody and was faint in 1-D BN-PAGE (**c**), while strong upon 2-D SDS-PAGE separation (**d**). Note, however, that the same secondary antibody reacted as expected against anti-complexin-I/II antibodies (i.e. SP33 and LP27, both IgG1), but not against anti-syntaxin-1 (i.e. SP7 IgG2a), in both 1-D and 2-D BN/SDS-PAGE. (**a**–**d**) Molecular masses (in kDa) of native and SDS-PAGE prestained standards are shown on the left and above.

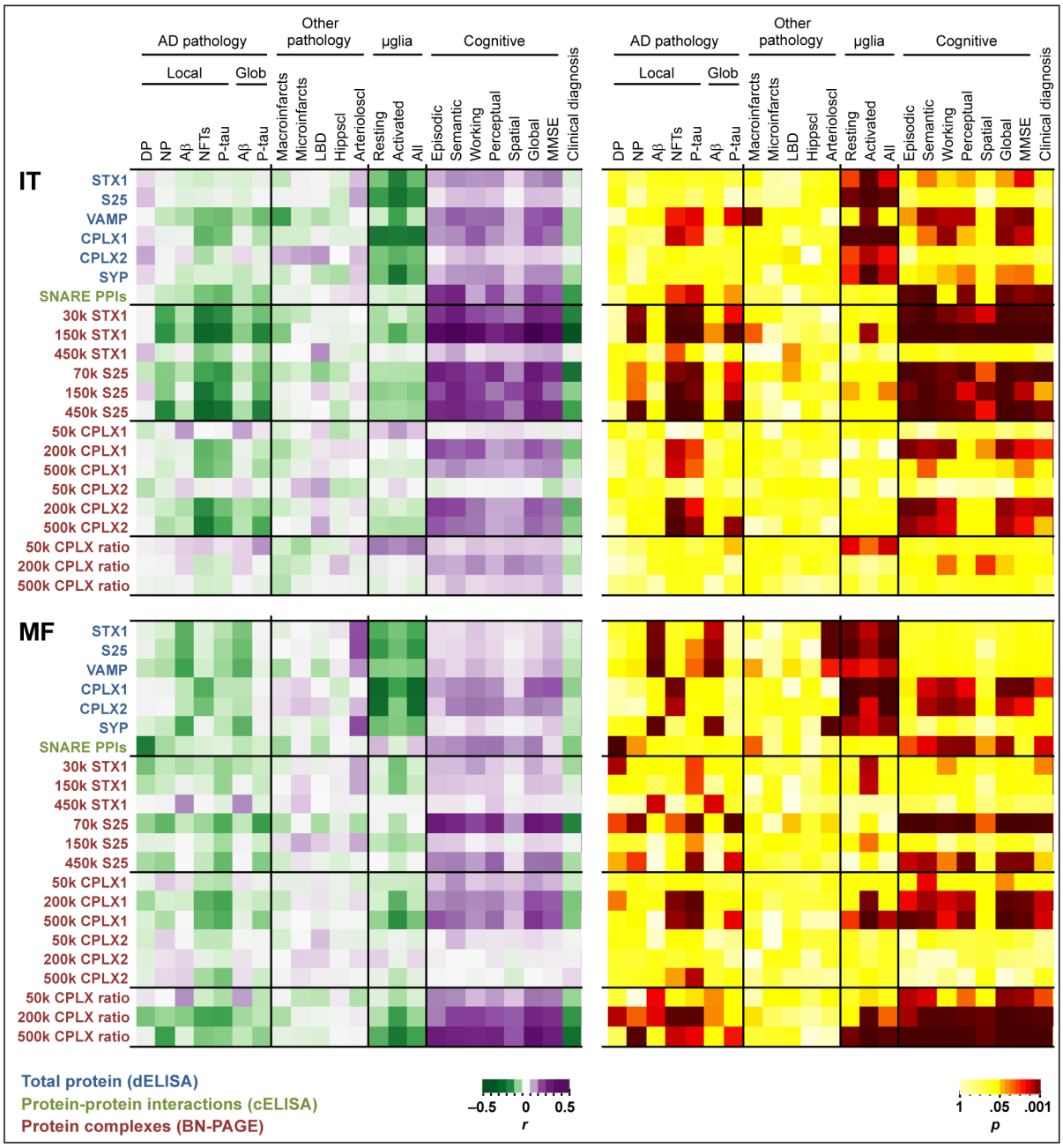

Fig. 2.

Heatmap of Pearson's *R* (left panel) and *P* (right panel) values following multiple pairwise correlations between the pathologic, stereological and cognitive variables of MAP participants on top, and the neurochemical data obtained in the inferior temporal (IT) or middle frontal (MF) gyri by either direct (d) or capture (c) ELISA, or BN-PAGE, as indicated on the left. The burden of both local (i.e. IT or MF) and global (Glob) brain AD (AD) pathology is evaluated. The ratios of complexin-I to complexin-II were also calculated for each of the equivalent BN-PAGE complexes as an index of functional inhibitory/excitatory input balance. For practical reasons, clinical diagnoses were coded as 0 (for NCI), 1 (MCI), or 2 (dementia). Abbreviations: Aβ, amyloid-β; Arterioloscl, arteriolosclerosis;

CPLX1, complexin-I; CPLX2, complexin-II; DP, diffuse plaques; Hippscl, hippocampal sclerosis; k, kDa (kilodaltons); LBD, Lewy body disease; μglia, microglia; MMSE, mini-mental state examination; NFT, neurofibrillary tangles; NP, neuritic plaques; P-tau, phosphotau; PPIs, protein-protein interactions; S25, SNAP25; STX1, syntaxin-1; SYP, synaptophysin; VAMP, vesicle-associated membrane protein.

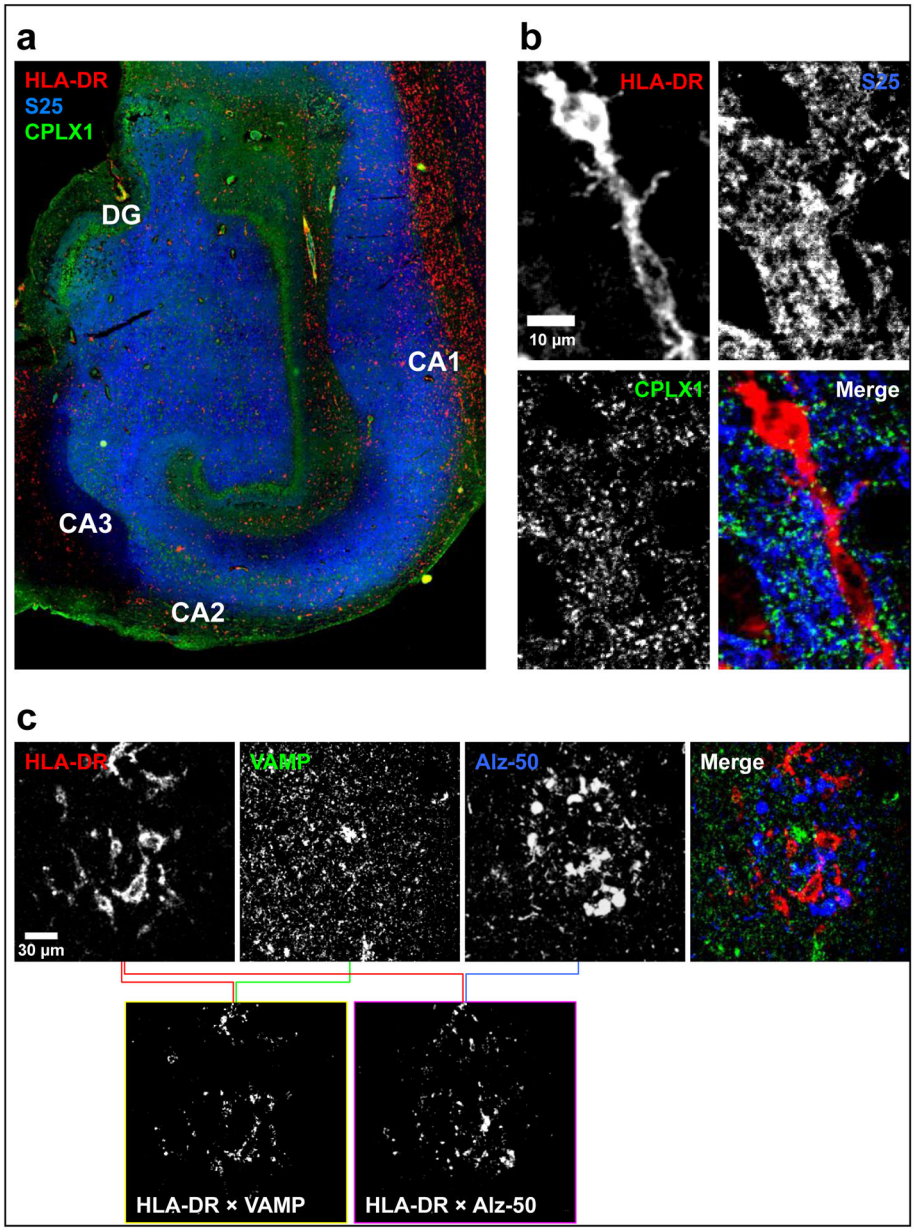

Fig. 3.

Representative images of human hippocampal sections in (**a**) epifluorescence and (**b** and **c**) confocal microscopy following triple immunostaining with antibodies against (**a** and **b**) HLA-DR (red; clone CR3/43; targeting activated microglia), SNAP25 (S25; blue; clone SP12) and complexin-I (CPLX1; green; clone SP33), or (**c**) HLA-DR (red), VAMP (green; clone SP10) and misfolded tau (blue; clone Alz-50). (**a**) Overview of the hippocampal subfields in a paraffin-embedded, 6-µm-thick section, showing the expected localizations for HLA-DR (activated microglia-like cells), SNAP25 (labeling the neuropil with strongest staining throughout the perforant pathway), and CPLX1 (intense staining of the neuropil attributable to GABAergic terminals surrounding granule cells of the dentate gyrus [DG] and pyramidal cells within the CA regions). (**b**) Example of a confocal micrograph of an HLA-

DR-positive cell with clear inclusions of presynaptic material, in a free-floating, 40-μm-thick hippocampal section. (**c**) Positive colocalization analysis of both VAMP and Alz-50 with HLA-DR, using the method by Costes *et al.* [41,43]. Upper panels are single or merged channel confocal images, while bottom panels are ImageJ-built bitmaps resulting from pairwise colocalization analyses between the indicated antibodies, and represent those pixels where the overlapping between the channels are above an unbiased threshold of intensities

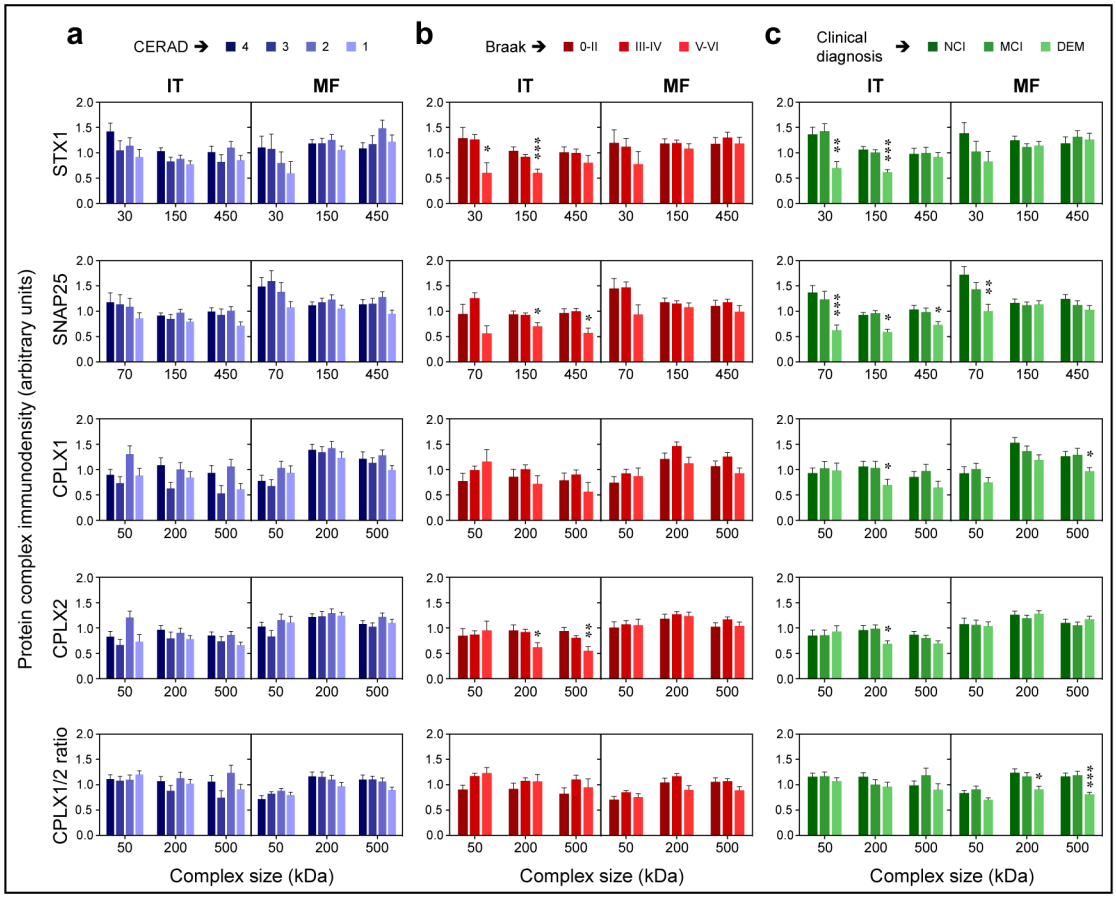

Fig. 4.

Temporal (IT) and frontal (MF) immnudensities of the major complexes quantified in the study in brains of MAP participants stratified by (**a**) CERAD scale, (**b**) Braak stage, or (**c**) clinical diagnosis. Bars are mean ± standard error. Datasets were analyzed by ANCOVA, using each protein complex measure as the dependent variable in separate models, CERAD/Braak/clinical diagnoses as the dependent variables, and sex, age, and PMI as covariates. *$P < 0.05$, **$P < 0.01$, and ***$P < 0.001$, FDR-corrected P-values in ANCOVA followed by Dunnet's *post hoc* test.

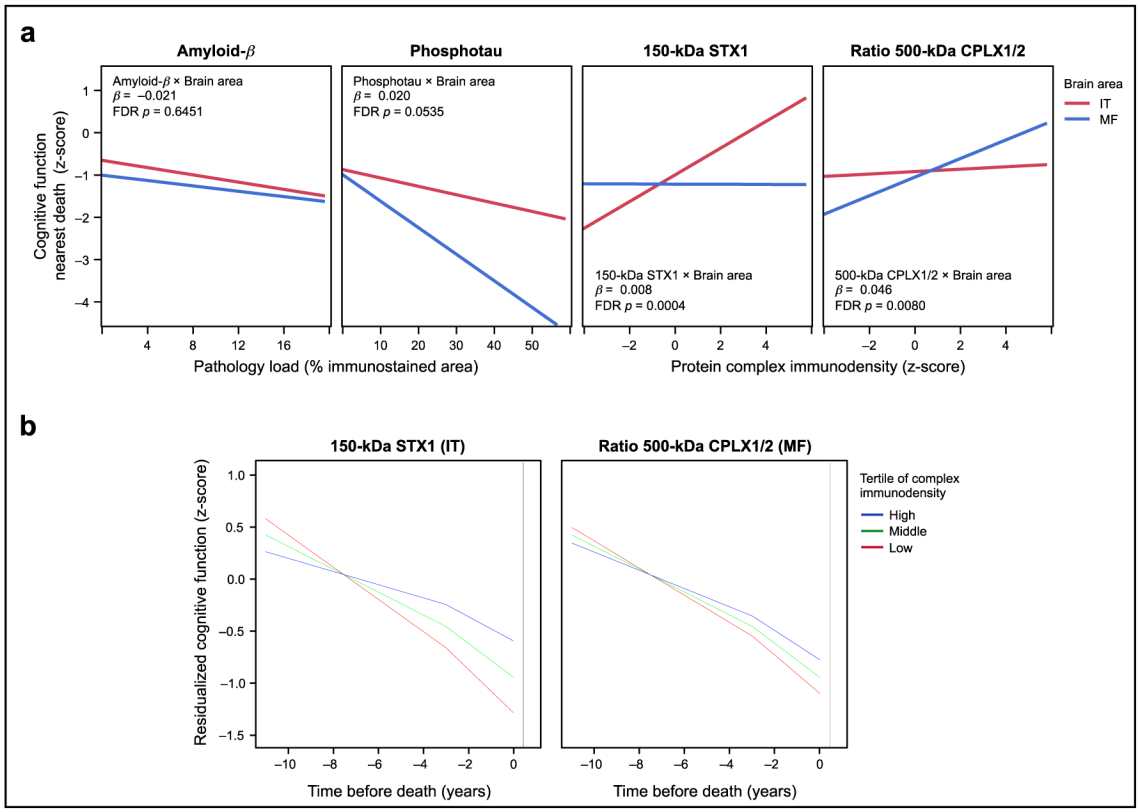

Fig. 5.

(**a**) Interaction plots resulting from the double dissociation model predicting MAP participants' cognitive function nearest death (and controlling for typical demographic and pathologic variables), in which the amounts of temporal (IT) and frontal (MF) pathologic (amyloid-β and phosphotau) and presynaptic function (150-kDa syntaxin-1 and 500-kDa complexin I/II ratio) indices were each crossed by a term identifying the brain area where they were measured. Lines represent the best fit for the association between cognition and the amounts of each of these brain indices in IT (red) and MF (blue). After false discovery rate (FDR) correction, the interaction terms of presynaptic indices by brain area were both highly significant, whereas those crossing the pathologic indices by brain area were not (beta-estimates and *p*-values for each interaction term are shown in each scatterplot; full model not shown). (**b**) Trajectory of cognitive decline (residual values after adjusting for demographics, neuropathologies, synaptic density and cognitive function nearest death) associated with MAP participants within the high (blue), middle (green), and low (red) tertiles of 150-kDa STX1 immunodensities in IT (left) or the 500-kDa CPLX1/CPLX2 ratio values in MF (right). Models included fixed change-point at 3 years prior to death indicating period of terminal cognitive decline.

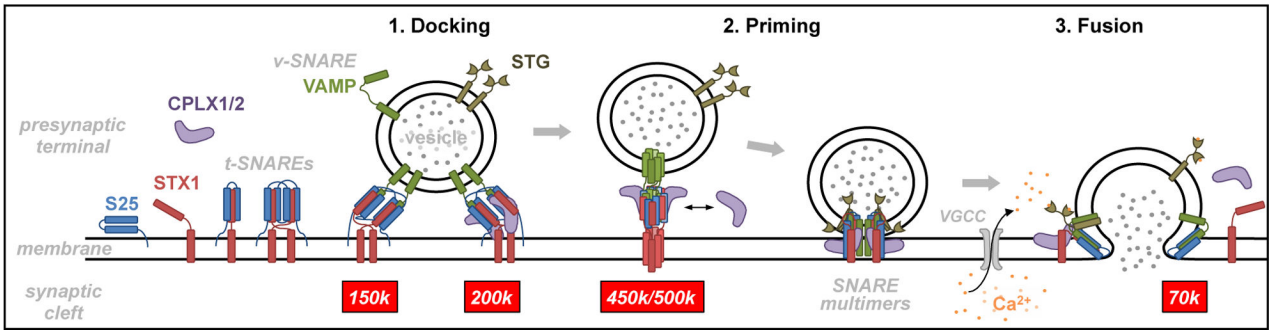

Fig. 6.

Cartoon summarizing the cycle of vesicle trafficking and neurotransmitter release, and the steps where the characterized and quantified protein complexes (tagged with their corresponding molecular weights in red boxes) are hypothesized to participate in the process. Abbreviations: CPLX1/2, complexins-I/II; *k*, kDa; S25, SNAP25; STG, synaptotagmin; STX1, syntaxin-1; t-SNARE, target SNARE; VAMP, vesicle-associated membrane protein; VGCC, voltage-gated calcium channel; v-SNARE, vesicle SNARE.

Table 1

Demographic, cognitive and pathological characteristics[a] of MAP participants with available samples from inferior temporal (IT) and/or middle frontal (MF) gyri

Variable	IT samples (*n* = 154)	MF samples (*n* = 174)	Both IT & MF (*n* = 140)	Any samples (*n* = 188)
Demographic				
Female, no. (%)	104 (68%)	119 (68%)	99 (71%)	124 (66%)
Age at death, years	88.6 ± 6.5	89.0 ± 6.2	88.6 ± 6.4	89.0 ± 6.2
Education, years	14.6 ± 3.0	14.6 ± 2.9	14.6 ± 3.0	14.6 ± 2.9
APOE ε4 carriers, no. (%)	34 (22%)	39 (22%)	32 (23%)	41 (22%)
PMI, hours	6.5 ± 3.5	6.9 ± 4.1	6.6 ± 3.6	6.8 ± 4.0
Cognitive function proximate to death				
Global cognition score	−0.78 ± 1.04	−0.79 ± 0.99	−0.77 ± 1.00	−0.80 ± 1.02
Episodic memory	−0.72 ± 1.15	−0.72 ± 1.13	−0.70 ± 1.13	−0.73 ± 1.15
Semantic memory	−0.60 ± 1.19	−0.61 ± 1.12	−0.57 ± 1.13	−0.63 ± 1.17
Working memory	−0.64 ± 1.09	−0.68 ± 1.02	−0.63 ± 1.05	−0.68 ± 1.06
Perceptual speed	−0.92 ± 0.98	−0.93 ± 0.97	−0.92 ± 0.99	−0.93 ± 0.97
Visuospatial ability	−0.59 ± 1.11	−0.68 ± 1.12	−0.65 ± 1.11	−0.63 ± 1.13
MMSE	21.7 ± 8.5	21.8 ± 8.3	21.9 ± 8.3	21.7 ± 8.4
Clinical diagnoses,[b] no. NCI:MCI:DEM	53:45:56	55:50:69	49:40:51	59:55:74
Pathological				
NIA/Reagan scale,[c] no. in 1:2:3:4	19:65:66:4	23:76:72:3	18:58:61:3	24:83:77:4
CERAD scale,[d] no. in 1:2:3:4	42:43:26:43	51:50:29:44	40:36:25:39	53:57:30:48
Braak stage,[e] no. in 0-II:III-IV:V-VI	32:92:30	31:106:37	26:86:28	37:112:39
Global amyloid pathology	3.71 ± 3.98	4.25 ± 4.42	3.64 ± 3.98	4.27 ± 4.49
IT amyloid pathology, % area stained	3.78 ± 4.09	4.38 ± 4.64	3.73 ± 4.11	4.37 ± 4.58
MF amyloid pathology, % area stained	5.16 ± 5.61	6.04 ± 6.32	5.07 ± 5.63	6.04 ± 6.24
Global tauopathy	5.99 ± 6.37	5.89 ± 6.16	5.90 ± 6.09	5.97 ± 6.39
IT tauopathy, % area stained	6.62 ± 11.9	6.63 ± 11.4	6.27 ± 10.6	7.06 ± 12.4
MF tauopathy, % area stained	1.07 ± 2.91	1.29 ± 3.72	1.13 ± 3.03	1.23 ± 3.59
IT diffuse plaques, counts/mm^2	9.1 ± 12.2	9.8 ± 12.4	9.2 ± 12.3	9.7 ± 12.3
MF diffuse plaques, counts/mm^2	10.0 ± 13.8	10.5 ± 14.0	9.8 ± 13.2	10.6 ± 14.4
IT neuritic plaques, counts/mm^2	9.2 ± 11.5	10.1 ± 12.4	9.3 ± 11.9	9.9 ± 12.1
MF neuritic plaques, counts/mm^2	7.8 ± 9.3	8.1 ± 9.5	7.6 ± 9.3	8.2 ± 9.5
IT NFTs, counts/mm^2	4.7 ± 10.1	4.7 ± 9.7	4.6 ± 9.8	4.8 ± 9.9
MF NFTs, counts/mm^2	1.4 ± 4.7	1.6 ± 4.8	1.5 ± 4.9	1.5 ± 4.6
Macroinfarcts, no. (%)	47 (31%)	54 (31%)	41 (29%)	60 (32%)
Microinfarcts, no. (%)	34 (22%)	42 (24%)	33 (24%)	43 (23%)
Lewy body disease, no. (%)	30 (19%)	29 (17%)	23 (16%)	36 (19%)
Hippocampal sclerosis, no. (%)	12 (8%)	12 (7%)	11 (8%)	13 (7%)
IT total microglia, counts/mm^2	147 ± 71	140 ± 68	137 ± 71	140 ± 68

Variable	IT samples (*n* = 154)	MF samples (*n* = 174)	Both IT & MF (*n* = 140)	Any samples (*n* = 188)
MF total microglia, counts/mm^2	167 ± 74	171 ± 71	167 ± 74	171 ± 70

Abbreviations: AD, AD; *APOE* ε4, Apolipoprotein E ε4 allele; CERAD, Consortium to establish a registry for AD; DEM, dementia; MAP, Memory and Aging Project; MCI, mild cognitive impairment; MMSE, mini mental state examination; NCI, no cognitive impairment; NFTs, neurofibrillary tangles; NIA, National Institute on Aging; no., number of subjects; PMI, postmortem interval; SD, standard deviation.

[a] Values are mean ± SD unless noted otherwise.

[b] Clinical diagnoses were obtained as indicated in the main text. Dementia group includes AD diagnoses and other dementias.

[c] NIA/Reagan scale: high (1), intermediate (2), low (3), or no (4) likelihood of AD, according to the presence and distribution of neuritic plaques and tangles.

[d] CERAD scale: frequent (1), moderate (2), sparse (3), or no (4) neuritic plaques.

[e] Braak staging: no or transentorhinal tauopathy (0-II), limbic spread (III-IV), or neocortical spread (V-VI).

Table 2

Linear regression models[a] showing the associations between most relevant presynaptic complexes identified in the IT and MF of MAP participants (n = 140), as predictors, and global cognitive function as the outcome

Model terms	Reference Model		Model 1		Model 2		Model 3	
	Adj. R^2 or β	FDR *P*-value	Adj. R^2 or β	FDR *P*-value	Adj. R^2 or β	FDR *P*-value	Adj. R^2 or β	FDR *P*-value
Model adj. R^2	0.3099		0.3991		0.3963		0.4398	
Age at death	−0.1681	0.0605	−0.1459	0.0797	−0.1882	0.02 02 *	−0.1663	0.03 40 *
Sex	0.0568	0.5450	0.0197	0.7854	0.0282	0.6972	0.0075	0.9144
Education	−0.1058	0.3606	−0.1084	0.2598	−0.1060	0.2775	−0.1079	0.2225
PMI	−0.0698	0.5450	−0.0555	0.7175	−0.0798	0.4498	−0.0665	0.5352
Macroinfarcts	−0.0513	0.5450	−0.0299	0.7854	−0.0459	0.6972	−0.0312	0.7007
Lewy bodies	−0.2647	0.0075 *	−0.2560	0.0027 *	−0.2353	0.0077 *	−0.2363	0.0068 *
Hippocampal sclerosis	−0.0190	0.8153	−0.0242	0.7854	−0.0361	0.6972	−0.0356	0.7007
p-amyloid[b]	−0.2475	0.0161 *	−0.2277	0.0136 *	−0.2336	0.0109 *	−0.2222	0.0102 *
Phosphotau[b]	−0.2276	0.0241 *	−0.1678	0.0797	−0.1925	0.0340 *	−0.1563	0.0852
Synapse density[c]	0.0710	0.5450	−0.0444	0.7414	0.0286	0.6972	−0.0476	0.6604
IT 150k STX1	–	–	0.3311	0.0002 *	–	–	0.2499	0.0068 *
MF 500k CPLX1/2 ratio[d]	–	–	–	–	0.3009	0.0002 *	0.2236	0.0068 *

Abbreviations: CPLX, complexin; FDR, false discovery rate; IT, inferior temporal gyrus; MF, middle-frontal gyrus; PMI, postmortem interval; S.E., standard error; STX1, syntaxin-1.

[a] Models 1–3 were constructed sequentially by adding the indicated terms to the reference model. Whole model adjusted R^2, individual standardized coefficients (β) and FDR-adjusted p-values are reported.

[b] Overall brain load.

[c] Synapse density was estimated as the overall brain levels of the three SNARE proteins (syntaxin-1, SNAP-25 and VAMP) averaged.

[d] Ratio between complexin-I (GABAergic) to complexin-II (glutamatergic) 500-kDa complexes.

* Statistically significant.